Ludmilla Derr; Nils Hildebrand; Susan Köppen; Simon Kunze; Laura Treccani;Ralf Dringen;Kurosch Rezwan;Lucio Colombi Ciacchi

Physisorption of α-chymotrypsin on SiO2 and TiO2: A comparative study via experiments and molecular dynamics simulations

Ludmilla Derr, Nils Hildebrand, Susan Köppen, Simon Kunze, Laura Treccani, Ralf Dringen, Kurosch Rezwan, Lucio Colombi Ciacchi; Physisorption of α-chymotrypsin on SiO2 and TiO2: A comparative study via experiments and molecular dynamics simulations. Biointerphases 1 March 2016; 11 (1): 011007. https://doi.org/10.1116/1.4940701

Physisorption of α-chymotrypsin on SiO_2 and TiO_2: A comparative study via experiments and molecular dynamics simulations

Ludmilla Derr; Nils Hildebrand; Susan Köppen; Simon Kunze; Laura Treccani; Ralf Dringen; Kurosch Rezwan; Lucio Colombi Ciacchi

Physisorption of α-chymotrypsin on SiO_2 and TiO_2: A comparative study via experiments and molecular dynamics simulations

Ludmilla Derr
Advanced Ceramics, Faculty of Production Engineering, University of Bremen, Am Biologischen Garten 2, Bremen 28359, Germany

Nils Hildebrand, Susan Köppen, and Simon Kunze
Hybrid Materials Interfaces Group, Faculty of Production Engineering and Bremen Center for Computational Materials Science, University of Bremen, Am Fallturm 1, Bremen 28359, Germany and MAPEX Center for Materials and Processes, University of Bremen, Bremen 28359, Germany

Laura Treccani
Advanced Ceramics, Faculty of Production Engineering, University of Bremen, Am Biologischen Garten 2, Bremen 28359, Germany

Ralf Dringen
Center for Environmental Research and Sustainable Technology, University of Bremen, Leobenerstraße NW2, Bremen 28359, Germany and Center for Biomolecular Interactions Bremen, University of Bremen, Leobenerstraße NW2, Bremen 28359, Germany

Kurosch Rezwan
Advanced Ceramics, Faculty of Production Engineering, University of Bremen, Am Biologischen Garten 2, Bremen 28359, Germany and MAPEX Center for Materials and Processes, University of Bremen, Bremen 28359, Germany

Lucio Colombi Ciacchi[a)]
Hybrid Materials Interfaces Group, Faculty of Production Engineering and Bremen Center for Computational Materials Science, University of Bremen, Am Fallturm 1, Bremen 28359, Germany; Center for Environmental Research and Sustainable Technology, University of Bremen, Leobenerstraße NW2, Bremen 28359, Germany; and MAPEX Center for Materials and Processes, University of Bremen, Bremen 28359, Germany

In order to understand fundamental interactions at the interface between immobilized enzymes and ceramic supports, the authors compare the adsorption features of chymotrypsin on SiO_2 and TiO_2 colloidal particles by means of a combination of adsorption experiments and molecular dynamics simulations. While the dependency of the adsorption amount on *p*H is consistent with the trend predicted the Derjaguin-Landau-Verwey-Overbeek theory, other effects can only be rationalized if the atomic-scale details of the water-mediated protein–surface interactions are considered. On both surfaces, a clear driving force for the formation of a double monolayer at the saturation coverage is found. Although nearly equal free energies of adsorption are estimated on the two materials via a Langmuir adsorption analysis, about 50% more proteins per unit of surface can be accommodated on TiO_2 than on SiO_2. This is probably due to the lower surface diffusion mobility of the adsorbed protein in the latter case. Surface anchoring is realized by a combination of direct ionic interactions between charged proteins and surface sites (more pronounced for SiO_2) and distinct structuring of the surface hydration layers in which the contact residues are embedded (more pronounced for TiO_2). Finally, normalization of the data with respect to particle surface areas accessible to the proteins, rather than determined by means of the Brunauer-Emmett-Teller nitrogen adsorption isotherm, is crucial for a correct interpretation of the results.

I. INTRODUCTION

Enzymes are widely exploited for industrial and technological applications as catalysts in complex chemical processes operating under mild environmental conditions. Since free and soluble enzymes pose several handling problems, they are often immobilized onto solid insoluble supports.[1–3] Immobilization confers enzymes higher stability toward temperature variations and solvents,[4–6] permits enzyme reusability in continuous processes,[7–9] facilitates their recovery after the reaction without any significant loss to its biochemical properties,[4,6] and allows an easier separation from other dissolved compounds.[4,10–13] Immobilization of enzymes on solid supports via covalent binding, entrapment, or adsorption via, e.g., hydrophobic and ionic interactions, may provide stability to the immobilized enzyme structure, ultimately resulting in an improved enzyme activity and stability.[4,6] Covalent binding permits a stable enzyme fixation to the carrier material and suppresses enzyme leaching. However, it often requires several synthesis steps including

surface conditioning with hazardous chemicals.[14] On the contrary, immobilization by physical adsorption is considered to be a more straightforward and therefore economically attractive and environment-friendly approach.[4,6,15] It does not require any additional chemicals and can be carried out at mild conditions.[16]

Numerous studies have focused on the application of ceramics such as silica (SiO_2) and titania (TiO_2) as solid supports or carrier materials in biotechnological applications.[17–22] These include bioreactors, water purification devices,[23–26] chromatography applications systems,[27] biomedical implants, and drug delivery systems.[17–19,22,28–30] It is well known that adsorption on hydrophobic materials may induce strong conformational changes of the adsorbed proteins, which could inactivate them.[31–33] On hydrophilic surfaces, adsorption is generally found to better conserve the native protein structure,[31–33] which makes ceramic particles suitable for technical use as an enzyme carrier material. SiO_2 and TiO_2, considered in this work, have different isoelectric points (IEPs) and different surface charge distributions. They are therefore representative candidates to carry out a fundamental study of noncovalent interaction mechanisms between their surfaces and adsorbed enzymes in aqueous solutions.[34] For our study, we have selected the well-characterized and technically relevant enzyme α-chymotrypsin. Chymotrypsin is a mammalian digestive enzyme involved in the proteolytic activity of pancreatic juice, and in the hydrolysis of peptide bonds,[32] specifically those in which the carbonyl group belongs to phenylalanine, tyrosine, or tryptophan amino acids.[35] Chymotrypsin is widely used both diagnostically and therapeutically for the treatment of pancreatic disease, and is involved in cancer metastases.[36–38]

Protein adsorption onto carrier materials is initially driven by van der Waals attraction combined with entropic repulsion or attraction of the diffuse ion layers between protein and surface [Derjaguin-Landau-Verwey-Overbeek (DLVO) interactions[39]] due to the presence of surface charges. Anchoring to the materials surface is then realized through solvent-mediated effects, hydrogen bonds, ionic bonds, and metal ion bridges.[5,34,40,41] The reported activity and the amount of adsorbed enzymes vary widely depending on the specific carrier material/enzyme pair.[32,33,42] Previous circular dichroism studies of chymotrypsin adsorbed on hydrophobic Teflon or on hydrophilic fumed SiO_2 performed by Zoungrana *et al.*[33] and Norde and Zoungrana[32] showed that chymotrypsin tends to build tightly packed adsorbed layers. On SiO_2, a clear loss of the helical content of the molecule due to the interaction with SiO_2 has been reported.[33] Nevertheless, the measured activity has been observed to diminish only slightly after adsorptions, suggesting an overall conservation of the tertiary protein structure in proximity of the enzymatically active site. This is consistent with the idea that globular proteins adsorb on solid particles forming a rather compact layer with thickness comparable to the dimension of the native molecule,[43] even though structural rearrangements could take place at the protein/surface interface region.

Regarding the strength of the protein/surface interactions, it has been shown that the binding affinity of proteins to particle surfaces do not correlate with their net charges, but rather depends on the mutual distribution of charged sites on either side of the interface.[44,45] For the case of chymotrypsin on SiO_2, Zoungrana *et al.*[33] and Welzel[46] were not able to desorb previously adsorbed molecules neither in phosphate buffer at *p*H 7.1 nor in 0.01 M sodium chloride solutions,[33] and interpreted the results in terms of a nonreversible adsorption.

Although several studies on enzyme physisorption on ceramic materials have been reported, the precise effects of different surfaces on the adsorption behavior of enzymes are still poorly understood. In this study, we perform a systematic comparison of the adsorption of chymotrypsin on SiO_2 and TiO_2 particles, taking into account environmental parameters such as *p*H, ionic strength, enzyme concentration, and incubation time. The obtained experimental results are rationalized by means of comprehensive molecular dynamics (MD) simulations that give insights into the adsorption orientation, surface diffusion mobility, and atomistic details of the protein–surface contact points. The combined experimental and simulation analyses elucidate the adsorption behavior of chymotrypsin from single molecules up to a dense protein layer at a saturation coverage corresponding to at least a double monolayer. In our analysis, we highlight the crucial role played by correct quantification of the particle surface area accessible to proteins, which we suggest to differ considerably from the one measured by conventional Brunauer-Emmett-Teller (BET) nitrogen adsorption. This is especially the case for microporous materials, such as some types of SiO_2 particles.

II. EXPERIMENTAL SETUP AND METHODOLOGY

A. Materials

Silica colloidal particles (SiO_2; SiO_2P015-01, >99.9 wt. %, Lot. No. 100618-02V) were obtained from Fibre Optic Center (USA). Titania colloidal particles (TiO_2; PT401L, 78 wt. % rutile and 22 wt. % anatase, Lot. No. 0108) were purchased from Ishihara Sangyo Kaisha, Ltd. (Japan). Lyophilized α-chymotrypsin type II from bovine pancreas (molar weight 25 300 g mol^{-1}, purity 94.1 wt. %, Lot. No. 60M7007V), *p*-nitrophenol acetate (CAS No. 830-03-5, Lot. No. 0001422901), potassium dihydrogen phosphate (≥99 wt. %, CAS No. 7778-77-0), sinapic acid (Lot. No 1392702 32008266), and 1,4-dioxan (>99.8 wt. %, CAS No. 123-91-1, Lot. No. STBB3939) were obtained from Sigma-Aldrich (Germany) and used without any modifications. Pierce™ bicinchoninic acid protein assay kit (BCA assay) was obtained from Thermo Fisher Scientific GmbH (Germany). All other chemicals were purchased from Fluka (Switzerland) or Merck (Germany) at analytical grade. For all aqueous solutions double deionized water (ddH_2O) with a conductivity of 0.04 μS cm^{-1} was used as the solvent (Millipore Synergy®, Millipore Corporation, Germany).

B. Characterization of SiO_2 and TiO2

Prior to each investigation, SiO_2 and TiO_2 particles were calcinated at 400 °C for 4 h with a heating and cooling rate of 3 °C min^{-1} (oven L3/11/S27, Nabertherm, Germany) to

remove any organic contaminants. Control thermogravimetric analysis confirms that no other adsorbants than water are present on the particles' surfaces after calcination (data not shown). The particle size was determined by dynamic light scattering (DLS, Beckman-Coulter DelsaNanoC, Beckman Coulter GmbH, Germany) using 0.003 vol. % SiO_2-suspension at *p*H 5 or 0.003 vol. % TiO_2-suspension at *p*H 3 (about 2–3 *p*H units away from the IEP, to reduce the tendency toward agglomeration). Prior to each DLS measurement, the suspensions' conductivity and *p*H were adjusted to avoid or to minimize particle agglomeration and the particle suspensions were deagglomerated for 10 min using an ultrasound sonotrode Sonifier® 450 (output 150 W, pulse rate 0.5 s, Branson, USA). Deagglomeration did not change any surface-specific property such as IEP. The suspension conductivity was set at 500 μS cm^{-1} using 3 M KCl, and *p*H was adjusted with 1 M KOH or 1 M HCl. The DLS measurements were performed at room temperatures. The resulting polydispersity indexes were approximately 0.06 for SiO_2 (indicative of monodispersity) and 0.18 for TiO_2 (indicative of moderate polydispersity, in agreement with the microscopic imaging).

The BET specific surface area (SSA_{BET}) was obtained by volumetric nitrogen adsorption measurements using a BELsorp-mini II device (BEL Japan, Japan) assuming a cross-sectional area of the nitrogen molecule of 0.162 nm^2.[32] The ζ-potential measurements were performed in 1 vol. % aqueous suspensions of SiO_2 and TiO_2 using the electroacoustic colloidal vibration current technique (Acoustic & Electroacoustic Spectrometer DT-1200, Dispersion Technology, USA) as described in Ref. 47. SiO_2 and TiO_2 suspensions with an initial conductivity of 500 μS cm^{-1} were titrated using 1 M KOH or 1 M HCl to measure the ζ-potential as a function of *p*H and to determine the IEP. The quantity of hydroxyl groups present on the surface of the colloidal particles was determined by titrations according to Hidber.[41,48]

The particle morphology was analyzed by scanning electron microscopy (SEM; field-emission SEM SUPRA 40, Zeiss, Germany) operating at 2.00 kV mounted on carbon tape, and by transmission electron microscopy (TEM) using a FEI Titan 80/300 kV (FEI, The Netherlands) equipped with a Cs-corrector for spherical aberration of the objective lens at 300 kV and a vacuum at 1.3×10^{-7} mbar. SiO_2 and TiO_2 particles were deposited on chemical vapor deposition graphene film coated copper grids (Graphene Supermarket, New York, USA). The geometrical particle sizes were obtained by superimposing circles on 20 randomly chosen particles in several different TEM images for each material and averaging over the different values (see supplementary material, Fig. S1).[49] The hydrophilic/hydrophobic surface properties were investigated by volumetric water vapor and *n*-heptane adsorption measurements using a BELsorp 18-3 device (Bel Japan, Inc., Japan).

C. MALDI-ToF-MS

Matrix-assisted laser desorption/ionization time-of-flight mass spectroscopy (MALDI-ToF-MS) was used to investigate the presence of self-digestion-derived peptides in the supernatants collected after chymotrypsin incubation for 20 h at *p*H 8. We used a MALDI-ToF-MS Voyager DE-Pro (Applied Biosystems, Foster City, USA) controlled by the VOYAGER CONTROL PANEL software. Measurements were carried out on polished steel targets, using a sinapic acid solution in an acetonitrile/ddH_2O mixture as the matrix. Spectra were recorded in linear mode at the mass ranges of 5–30 kDa and 10–100 kDa to see the typical patterns associated with the chymotrypsin monomer and the possible presence of the chymotrypsin dimers. In order to achieve statistically relevant results, 100 shots per position were taken. Furthermore, measurements were repeated at three different positions within the spotted sample and accumulated. To investigate a possible time-dependent autolysis of chymotrypsin, MALDI-ToF-MS measurements were performed in the low measuring range of 800–5000 Da at incubation start, after 1, 4, and 20 h of incubation. Prior to the measurements, an external calibration was carried out using the calibration mixtures CalMixI and CalMixII, according to the manufacturer's instructions.

D. Time- and *p*H-dependent adsorption of chymotrypsin to SiO_2 and TiO_2

Aqueous suspensions (1 vol. %) of SiO_2 and TiO_2 particles were prepared by mixing 1.3 g of SiO_2 or 2.12 g of TiO_2 with 49.5 ml of ddH_2O. The values of density used for the calculation are given in Table I. The *p*H was adjusted using 1 M HCl or 1 M KOH solutions to *p*H 3, 5, 7.4, or 8, and the suspension conductivity was set to 500 μS cm^{-1}, which corresponds to an ionic strength of 3 mM, using 3 M KCl. Prior to incubation with chymotrypsin, the particle suspensions were deagglomerated for 10 min using an ultrasound sonotrode Sonifier® 450 (output 150 W, pulse rate 0.5 s, Branson, USA). Chymotrypsin stock solution (concentration of 20 mg ml^{-1}) was freshly prepared by dissolving chymotrypsin in ddH_2O, and the *p*H was adjusted as described before.

Incubation was carried out by mixing 900 μl of particle suspension with 100 μl chymotrypsin stock solution in 1.5 ml polypropylene tubes (Eppendorf AG, Germany). Precipitation was prevented by permanent overhead shaking (Stuart rotator STR4, Bibby Scientific, Ltd., UK) at a speed of 30 rpm at room temperature for 1, 4, or 20 h. The suspensions were centrifuged for 10 min at 21 100*g* (Heraeus Fresco 21 centrifuge, Fisher Scientific, Germany). Chymotrypsin concentrations in the supernatants and in chymotrypsin reference solutions without colloidal particles were measured with the BCA assay[52–55] with the lowest detection limit of 5 μg ml^{-1} according to the manufacturer's instructions. The enzymatic activity of chymotrypsin was determined according to Refs. 56–58. Briefly, 20 μl of the supernatant was mixed with 140 μl 100 mM potassium phosphate buffer in a well of a 96-microtiter plate (Nunc™, Denmark). The reaction was started by the addition of chymotrypsin substrate, 160 μl 0.2 mM p-nitrophenol acetate. The increase in absorbance due to the

TABLE I. Properties of SiO_2 and TiO_2 colloidal particles. All measured data represent means ± standard deviation of values that were obtained in three independent experiments. Theoretically calculated values are calculated as average of 20 values and reported with their standard deviation.

Property	SiO_2	TiO_2	Method
Purity[a] (wt. %)	≥99.9	≥99.9	—
DLS size (nm)	d_{50}: 180 ± 3	d_{50}: 384 ± 3	Dynamic light scattering
TEM size (nm)	142 ± 7	130 ± 15	TEM images
Specific surface area (SSA_{BET}) ($m^2\ g^{-1}$)	34.0 ± 0.3	12.4 ± 0.5	Volumetric nitrogen adsorption
Theoretical protein accessible surface area (PAA_{TEM}) ($m^2\ g^{-1}$)	12.8 ± 0.8	8.6 ± 1.0	Geometrical analysis of the TEM images
Exchange capacity (OH nm^{-2})	4.9 ± 0.2	0.6 ± 0.1	Titrations according to Hidber (Refs. 41 and 48)
IEP	2.7 ± 0.1	6.6 ± 0.1	Electroacoustic colloidal vibration current technique
Hamaker constant (Refs. 50 and 51) ($\times 10^{-21}$ J)	1.6	Rutile: 60 anatase: 37	Full spectral method
Density (g cm^{-3})	2.6 ± 0.1	4.2 ± 0.1	Pycnometer
Crystal structure	Amorphous	Rutile: 78 anatase: 22 wt. %	X-ray diffraction and electron diffraction with HR-TEM

[a]The data were given by the manufacturer.

formation of p-nitrophenolate ion was measured at 405 nm using a microtiter plate reader (Sunrise, Tecan, Austria).

E. Concentration-dependent adsorption of chymotrypsin to SiO_2 and TiO_2

The incubation was performed by mixing 900 μl of particle suspensions with 100 μl chymotrypsin stock solution reaching the start chymotrypsin concentrations of 0.22, 0.55, 0.69, 2.37, 4.95, and 6.85 mg ml^{-1}. After an incubation time of 20 h, the chymotrypsin concentration and the enzymatic activity in the supernatant were measured as previously described.[59] The experimental data were fitted using the Langmuir isotherm[60,61]

$$\Gamma = \frac{\Gamma_{\max} \times c}{K_L^{-1} + c}.$$

Here, Γ and $\Gamma_{\max}$ are the adsorbed and maximal adsorbed quantities, respectively, c is the chymotrypsin concentration in solution, and K_L is the Langmuir constant. The Gibbs energy of adsorption ΔG^0_{ads} can be estimated from the Langmuir constant[60,61] as

$$\Delta G^0_{ads} = -RT \times \ln\left(\frac{c_{solv}}{K_L^{-1}}\right),$$

where R is the gas constant, T is the temperature, and c_{solv} is the molar concentration of pure water (55.5 mol l^{-1}). The nonlinear least squares fit was performed by means of a Levenberg–Marquardt algorithm using SciPy.[62] The correlation of the nonlinear fit with the experimental data was quantified with a Pearson's correlation coefficient calculated by the scipy.stats.pearsonr function included in SciPy.[62]

F. Desorption studies

To test whether adsorption was reversible or irreversible, desorption studies with several washing steps were performed. To this aim, supernatant and colloidal particles were separated, and ddH_2O was added to the particles at the same *p*H as during the previous incubation. As before, the conductivity of H_2O was set at 500 μS cm^{-1} using 3 M KCl and *p*H was adjusted with 1 M KOH or 1 M HCl at the needed *p*H. After short rinsing, the supernatant was collected. This procedure was repeated three times. All the supernatants were used to measure the amount of adsorbed protein.

G. Molecular dynamics simulations

The protein structure for the performed simulations was taken from the Brookhaven Protein Database (PDB-ID: 4CHA). Missing residues and atoms were added to the protein monomer with the LEaP program (Link, Edit and Parm, which is included in the AmberTools simulation package at http://ambermd.org).[63] The size of the enzyme was approximated as a rectangular cuboid with edge lengths of 4.4, 4.7, and 5.0 nm in x, y, and z directions. The secondary structure of chymotrypsin comprises for the major part beta sheets, but presents two alpha helix motifs located on one side of the protein [Fig. 1(a)]. The enzymatically active site includes a triad of amino acids (serine 195, histidine 57, and aspartic acid 102),[64] which is highlighted in cyan in Fig. 1(a).

The "constant-*p*H" feature of the AMBER package[63] was used to adjust the protonation state of all titratable amino acids of the protein to the *p*H 3, 5, 7.4, and 8. The isoelectric point of chymotrypsin ranges between 8.5 and 8.8.[56,65–67] At our experimental conditions at $3 < pH < 8$, chymotrypsin has an overall positive charge. The distribution of the electrostatic potential around the protein was calculated by a numerical solution of the Poisson-Boltzmann equation using the "PBSA" program included in the AMBER package.[63] Consistently with the experiments, in the implicit-solvent simulations, the salinity was set to 3 mM, including monovalent ions only, and the temperature was set to 300 K. The electrostatic potential around chymotrypsin at *p*H 3, 5, 7.4, and 8 is represented in Figs. 1(b)–1(d) by negative (red) and positive (blue) isovalue surfaces at ±26 mV. At *p*H 3, chymotrypsin has a positive net charge of +7 e, giving rise to a predominantly positive potential surface, especially on one protein side. The net charge decreases to +4 e at *p*H 5 and +3 e at *p*H 7.4 and 8, resulting in the formation of separated positive (bottom) and negative

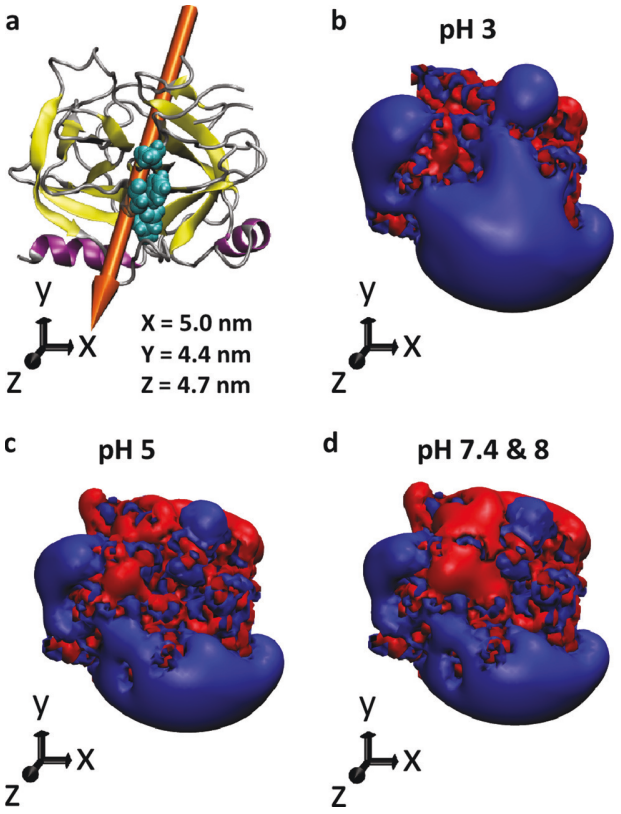

FIG. 1. (a) Schematic view of chymotrypsin. The catalytic triade is displayed in cyan spheres, the α-helices in purple, and the β-sheets in yellow. The molecular dipole is shown as an orange arrow. [(b)–(d)] Isosurfaces representing the calculated electrostatic potential around the protein at the values of $-1k_BT/e$ (−25.85 mV) (red) and $+1k_BT/e$ (+25.85 mV) (blue) at *p*H 3.0 (b), 5.0 (c) and 7.4 or 8.0 (d).

(top) protein regions. Accordingly, a strong dipole moment of 529 D ($1.76\ 10^{-27}$ C m) is oriented toward the positive end, directly facing the alpha helix region and is shown as an orange arrow in Fig. 1(a).

The protein is equilibrated for ∼1 ns in explicit solvent using the TIP3P water model.[68] The charge of the simulation cell is balanced including an appropriate number of chlorine ions (7, 4, or 3 at the different *p*H, see above). The final bare protein structure is taken for further simulations. The parameters for the simulation of the protein, ions, and the TIP3P water model are taken from the AMBER_99SB force field.[63] The amorphous structure of the $9 \times 9\,nm^2$ SiO_2 slab is taken from Cole *et al.*[69] To adjust the surface charge according to the *p*H, the protonation state of the surface terminal groups is changed as described by Butenuth *et al.*[70] The surface charges used in this work are average values of the results of potentiometric titration experiments.[61–74] This results in a final surface charge density of 0.0, −0.005, −0.05, and $-0.07\,C\,m^{-2}$ at *p*H 3.0, 5.0, 7.4, and 8.0, respectively, corresponding to 0, −5, −49, and −72 e, respectively, on the two slab sides.

A $8.1 \times 9.5\,nm^2$ slab model for an amorphous TiO_2 surface was created by cutting a single rutile crystal in an arbitrary direction, relaxing the surface atoms and annealing at 500 K for 200 ps to heal surface defects. The surface was then immersed in water. Water molecules next to undercoordinated Ti atoms with a coordination number smaller than five were dissociated by adding an OH-group to the Ti atom and binding the remaining proton to a neighbor bridging oxygen as described in Ref. 75 for the creation of TiO_2 particles. Terminal OH groups on Ti atoms and protonated bridging O atoms were considered as potential protonation/deprotonation sites, as described by a modified multisite complexation (MUSIC) model[76] by Köppen and Langel[77] (Fig. 2), resulting in a surface charge density of 0.113, 0.037, −0.055, and $-0.078\,C\,m^{-2}$ at *p*H 3.0, 5.0, 7.4, and 8.0, respectively (corresponding to +55, +18, −27, and −38 e, respectively, on one slab side). The intramolecular interactions among the TiO_2 crystal atoms were described by the force field developed in Ref. 78, while the intermolecular interactions of the TiO_2 atoms with water and biomolecules were described by the force field developed in Ref. 79.

The complete simulated systems consisted of one or multiple proteins above each of the two surfaces. The static calculations were performed in implicit solvent according to the Onufriev–Bashford–Case Generalized Born model[80] starting from 36 different protein orientations. The height of the protein over the surface was defined as the distance between the closest two atoms of surface and protein in the normal direction of the surface. No periodic boundary conditions were used. Therefore, the surface dimensions ($18.1 \times 18.1\,nm^2$ for the SiO_2 surface and $16.2 \times 19.1\,nm^2$ for the TiO_2 surface) were set large enough to avoid spurious edge effects. The distance cutoff of the nonbonded interactions was set to 100 nm. Force-distance profiles were evaluated for 36 different orientations of the protein from surface contact up to 5 nm above the surface in steps of 0.2 Å.

The molecular dynamics simulations were performed at 300 K in explicit TIP3P water molecules under periodic boundary conditions using the GROMACS simulation package[81]

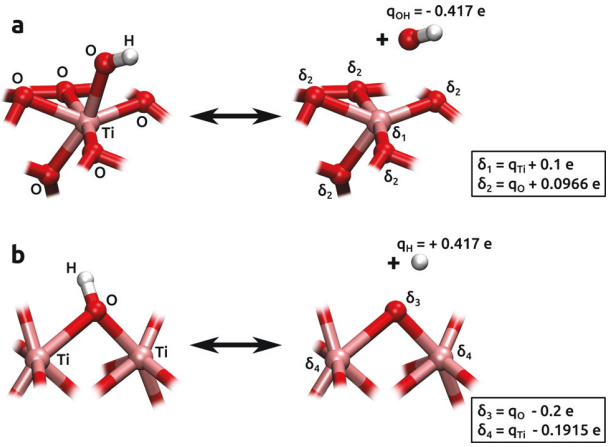

FIG. 2. Equilibrium of charged surface groups on TiO_2. Partial charges q_i are computed as described in Refs. 78 and 79. Local changes of the charges δ_i after protonation/deprotonation are indicated on the right. (a) Dehydroxylation of a terminal Ti-OH group, resulting in a total surface charge change of −1 e. (b) Deprotonation of a bridging OH group resulting in a total surface charge change of +1 e.

(version 4.5.5). The electrostatic interactions were treated with the smooth particle-mesh Ewald summation method. The size of the simulation box was chosen to ensure a separation distance of at least 4.5 nm between single proteins and their periodically repeated images in each case. A dense protein layer with a total surface density of 0.077 proteins nm^{-2} over TiO_2 and 0.073 proteins nm^{-2} over SiO_2 was placed as the initial structure over the respective surfaces. The orientations of the individual proteins were randomized. The charge was neutralized by an appropriate number of Na^+ ions, namely, 35 for single chymotrypsin on titania, 69 for single chymotrypsin on silica, and 20 for the multiprotein simulations. In the explicit-solvent MD simulations, the resulting salinities are therefore larger than the experimental value (3 mM). However, the resulting error is negligible, since monovalent ions do not mediate directly the surface/protein interactions. The water density was adjusted to that of TIP3P water at 300 K, namely, 0.983 g cm^{-3}. All surface atoms except the terminal OH groups were constrained in their equilibrium positions. In order to use a time step of 2 fs, the hydrogen atoms in the system were treated by the "linear constraint solver" algorithm.[82] The temperature in the dynamic simulation was adjusted with a modified Berendsen thermostat with an additional stochastic term that enables a correct canonical ensemble.[83] The coupling constant was set to 1 ps and the nonbonded interaction cutoff to 1.2 nm. Visualization analyses were performed with the Molecular Visualization program VMD.[84] The amount of secondary structure elements of the dissolved and adsorbed proteins was quantified using the Define Secondary Structure of Proteins method of Kabsch and Sander.[85]

III. RESULTS

A. Characterization of SiO_2 and TiO_2 colloidal particles

We begin our study with a detailed characterization of the used SiO_2 and TiO_2 colloidal particles, which is essential to interpret correctly the later presented protein adsorption experiments. The particle properties are summarized in Table I, and SEM and HR-TEM images are reported in Fig. 3 as well as in Fig. S1. These reveal almost perfectly spherical SiO_2 particles with an average diameter of 150 nm and agglomerates of more irregular TiO_2 primary particles with an average diameter of 130 nm, obtained approximating the irregular particles with spheres (Fig. S1). On the other hand, dynamic light scattering measurements give diameters for TiO_2 particles twice as large as those of SiO_2 particles (384 vs 180 nm, respectively). This could be due to the formation of TiO_2 agglomerates, which are probable according to the significantly higher Hamaker constant of TiO_2 (Table I). To ensure particle suspension, all probes are ultrasonicated. Despite the similar primary particle sizes visible in the SEM and HR-TEM images, the specific surface area (SSA_{BET}) determined by nitrogen adsorption is three times higher for SiO_2 (34.0 m^2 g^{-1}) than for TiO_2 (12.4 m^2 g^{-1}) (Table I). Instead, if spherical particle shapes are assumed in both cases, less dissimilar values or 12.1 and 8.6 m^2 g^{-1} are obtained for SiO_2 and TiO_2, respectively. We believe the larger SiO_2 BET surface area to be a consequence of the microporous structure of the Stöber silica material.[86,87] This would also explain the dramatically higher adsorption capacity and the hysteresis visible in the water adsorption isotherm of SiO_2 compared to TiO_2 (Fig. 4). Also, the values of proton exchange capacity (given in OH-groups per nm^2) are by a factor of 8 higher for SiO_2 than for TiO_2 (see Table I). Both surfaces, however, are predominantly hydrophilic, as revealed by the significantly smaller affinity to *n*-heptane than to water for both particle species. Concerning the adsorption of larger biomolecules such as chymotrypsin, we define here a protein accessible area based on the geometrical analysis of the TEM images (PAA_{TEM}, see Table I), assuming that the proteins cannot diffuse into the smaller micropores accessible instead to N_2 and H_2O molecules. This distinction between SSA_{BET} and PAA_{TEM} will be important to correctly interpret the formation of dense protein layers on the particle surfaces, as described in Sec. III B.

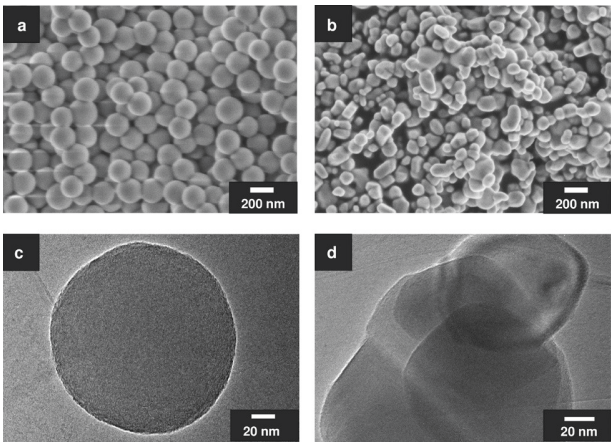

FIG. 3. Typical SEM [(a) and (b)] and HR-TEM [(c) and (d)] images of the employed SiO_2 [(a) and (c)] and TiO_2 [(b) and (d)] colloidal particles.

B. Dependence of the protein adsorption on incubation time and *p*H

The amount of chymotrypsin adsorbed on the SiO_2 and TiO_2 particles is measured as a function of the incubation time (1, 4, and 20) and solution *p*H (3, 5, 7.4, and 8) via two methods. Namely, both the concentration of protein remaining in solution after prolonged incubation and its enzymatic activity are determined and reported in Fig. 5. Immediately evident is the decrease in solution concentration of the enzyme at increasing *p*H values for both particles. This is consistent with previous studies[59] and indicates preferred adsorption of chymotrypsin on negatively charged surfaces. Concerning the incubation time, statistically insignificant variations are observed between 1 and 4 h, but a significant reduction in concentration is observed after 20 h for the case of SiO_2 at the higher *p*H values. This is in line with previous reports showing that an equilibrium adsorption coverage on hydrophilic SiO_2 is reached after about 16 h.[33,88,89]

The quantification of enzymatic activity in the supernatant follows a very similar trend. The used initial concentration of

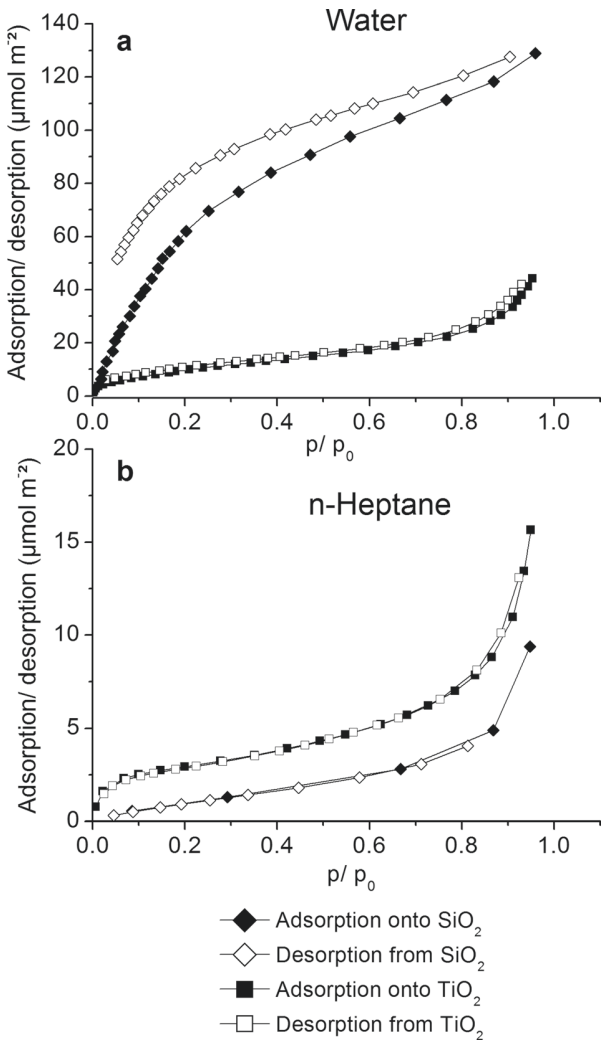

FIG. 4. Adsorption isotherms of (a) water and (b) *n*-heptane on SiO_2 and TiO_2 colloidal particles, normalized to their SSA_{BET} surfaces.

about 2 mg ml^{-1} results in a reference absolute activity of about 20 nmol *p*-nitrophenol min^{-1} ml^{-1} [Fig. 5(d)]. During incubation with the particles, the activity diminishes with increasing *p*H and incubation time. Here, it must be mentioned that the activity of the chymotrypsin reference solution itself is reduced by up to 30% after 20 h of incubation at higher *p*H. Thus, the dramatic supernatant activity reduction in the presence of particles is also due to aging effects, such as partial protein denaturation or blocking of the enzymatically active sites by organic contaminants, and not solely due to surface adsorption.

These combined measurements suggest a strong binding affinity of chymotrypsin to both SiO_2 and TiO_2 particles at neutral or basic *p*H. The affinity seems to be stronger for the case of TiO_2, for which the enzymatic activity of the supernatant was not measurable anymore after 20 h of incubation. Binding to SiO_2 seems to proceed via a slower kinetics, given the differences observed between 4 and 20 h of incubation. Repeated washing of the particles after chymotrypsin adsorption was not sufficient to remove a protein amount measurable with BCA assays (data not shown), suggesting an irreversible adsorption behavior on the time scale of the performed experiments. Finally, aging of the protein solution leads to a reduced enzyme activity also in the absence of particles. Whether this is caused by autolysis or by other effects is investigated in Sec. III C by means of MALDI-ToF-MS.

C. MALDI analysis of possible autolysis

The possible autolysis of chymotrypsin in solution and in the supernatant of TiO_2 and SiO_2 particle suspension is analyzed by means of MALDI-ToF-MS measurements at *p*H 8, where autolysis is most favorable.[35,90,91] The collected spectra are reported in Fig. 6 in the m/z ranges from 5 to 30 kDa and 10 to 100 kDa, and in supplementary Fig. S2 in the range of 800–5000 Da. In the spectra, the typical peaks arising from chymotrypsin monomers (around 25.2 kDa) and dimers (50.5 kDa) are well visible. Moreover, peaks of multiply charged proteins occur at around 12.6 and 6.3 kDa/charge

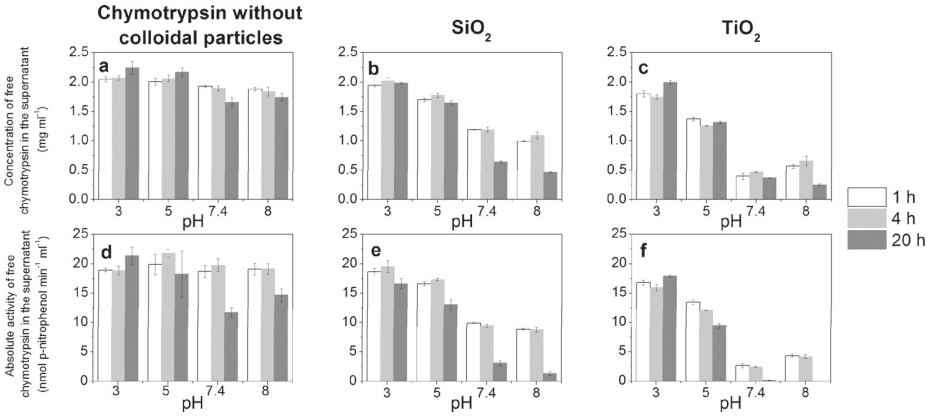

FIG. 5. Time and *p*H dependence of the concentration in the supernatant [(a)–(c)] and the absolute enzymatic activity in the supernatant [(d)–(f)] of chymotrypsin reference solutions [(a) and (d)] and after incubation with SiO_2 [(b) and (e)] and TiO_2 [(c) and (f)] colloidal particles. The data shown represent means ± SD of values obtained in three independent experiments with a starting chymotrypsin concentration of 2.0 mg ml^{-1} prior to *p*H adjustment [see panel (a)].

unit. Notably, no peaks attributable to peptide fragments derived from autolysis could be observed, irrespective of the incubation time and the absence or presence of particles (Fig. S2), consistently with a previous study.[92] In summary, this investigation confirms that the protein remains complete within the time scale of our experiments, and that the chymotrypsin monomer is by far the predominant species present in the used solutions.

D. Analysis of the adsorption layers

The amount of adsorbed chymotrypsin monomers can be now computed from the data shown in Fig. 5, subtracting the measured concentration in the supernatant from the initial concentration prior to incubation [Figs. 7(a)–7(d)]. Normalization of the adsorbed protein amount to the particle surface is performed considering both the SSA_{BET} and the PAA_{TEM} surfaces (see Table I), as anticipated above. As references for a side-on or an end-on monolayer, we consider rectangular surface units along the two main directions of the protein's envelope, corresponding to 25.0 and 19.4 nm^2 occupied by a single protein, respectively [see scheme in Fig. 7(e)]. The amount of adsorbed protein (given both as protein number per nm^2 and as protein mass per cm^2) is reported as a function of the *p*H and incubation time.

Using SSA_{BET} to normalize to the particle surface, the amount of chymotrypsin adsorbed onto TiO_2 appears to be almost twice as high as onto SiO_2 [Figs. 7(a) and 7(b)]. Namely, the data obtained after 20 h of incubation increased from 25 ng cm^{-2} at *p*H 3 to 160 ng cm^{-2} at *p*H 8 on SiO_2 [Fig. 7(a)], while on TiO_2 the adsorbed concentration varied from a minimum of 50 ng cm^{-2} at *p*H 3 to 310 ng cm^{-2} at *p*H 7.4 and 8 [Fig. 7(b)]. These values would correspond to a double layer of side-on adsorbed proteins on TiO_2 and to a single side-on layer on SiO_2. Simple arguments cannot explain this difference, especially given the considerably larger surface charge and water affinity of SiO_2 with respect to TiO_2, two properties that often correlate with the protein adsorption affinity. However, considering the PAA_{TEM} as the normalizing particle's surface, the situation changes. In this case, the maximum amount of adsorbed chymotrypsin is only slightly larger for TiO_2 (460 ng cm^{-2} at *p*H 7.4 after 20 h of incubation) than for SiO_2 (440 ng cm^{-2} at *p*H 8 after 20 h of incubation) [Figs. 7(c) and 7(d)]. As an important difference between the two materials, we note the continuous increase in adsorbed protein amount with *p*H on SiO_2, while the adsorption maximum is reached already at *p*H 7.4 for TiO_2. Other subtle differences such the variations of the adsorbed amount on TiO_2 between *p*H 7.4 and 8.0, being of the same order as the error bars, are probably insignificant and shall not be discussed in further detail.

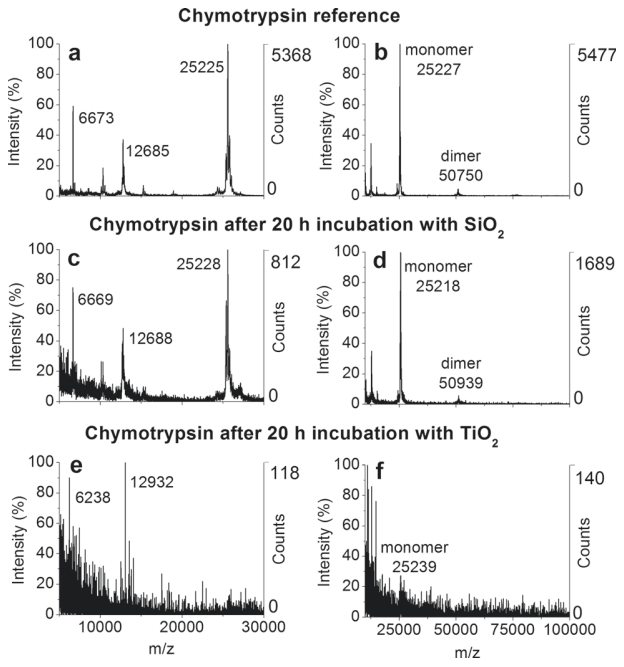

FIG. 6. MALDI-ToF-MS spectra of [(a) and (b)] the chymotrypsin reference, and of chymotrypsin after 20 h incubation at *p*H 8 with SiO_2 [(c) and (d)] or TiO_2 [(e) and (f)]. The spectra are shown for the m/z ranges from 5 to 30 kDa/e [(a), (c), and (e)], and from 10 to 100 kDa/e [(b), (d), and (f)].

E. Dependence of the adsorbed amount on the protein concentration

To investigate the dependence of the amount of adsorbed chymotrypsin on the initial concentration in solution, chymotrypsin is incubated with SiO_2 and TiO_2 at *p*H 8 in concentrations ranging from 0.22 to 6.85 mg ml^{-1} for 20 h. After incubation, the concentration in the supernatant is measured, and, by subtraction, the adsorbed concentration is determined. The results are reported in Fig. 8 considering both the SSA_{BET} and PAA_{TEM} surfaces for normalization, and are fitted with Langmuir isotherms to estimate the saturation adsorption amounts Γ_{max} and the free energies of adsorption ΔG^0_{ads}. For both particles types, saturation is reached in correspondence of supernatant concentrations of about 2 mg ml^{-1}. Consistently with the analyses in Sec. III D, more protein is found adsorbed on TiO_2 than on SiO_2. Namely, considering the SSA_{BET}, the values differed by a factor of three ($\Gamma_{max} = 488 \pm 65$ ng cm^{-2} for TiO_2 and $\Gamma_{max} = 155 \pm 18$ ng cm^{-2} for SiO_2), whereas the difference is less dramatic if normalization is performed with the PAA_{TEM} surface ($\Gamma_{max} = 700 \pm 103$ ng cm^{-2} for TiO_2 and $\Gamma_{max} = 436 \pm 58$ ng cm^{-2} for SiO_2). These values again correspond to adsorption well beyond a monolayer and indicate important differences in the adsorption modes of chymotrypsin on the two different surfaces. Interestingly, ΔG^0_{ads} (which is independent on the surface normalization) is almost the same for both materials, amounting to -34.3 ± 1.0 kJ mol^{-1} for TiO_2 and $= -35.6 \pm 1.0$ kJ mol^{-1} for SiO_2. Possible reasons leading to these effects are investigated by means of all atom molecular dynamics simulations in Sec. III F.

F. Long-range interaction force of chymotrypsin over SiO_2 and TiO_2

From the experiments described above, the amount of adsorbed protein on TiO_2 is either three times (SSA_{BET}) or

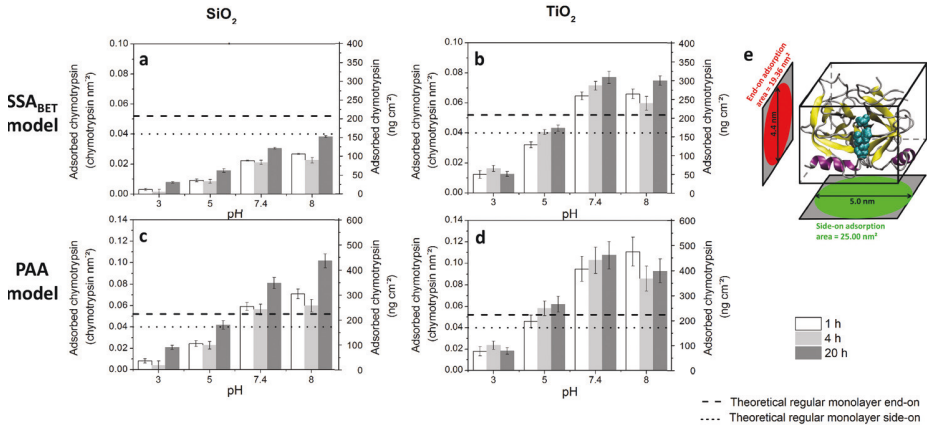

FIG. 7. Amount of chymotrypsin adsorbed on SiO_2 [(a) and (c)] and TiO_2 [(b) and (d)] as a function of time and *p*H. The data are expressed both in terms of ng/cm^2 and of number of molecules per nm^2 (right and left vertical axes in each panel, respectively). The concentration data are normalized to the SSA_{BET} [(a) and (b)] or the PAA_{TEM} [(c) and (d)] surface areas (see Table I and text). Theoretically calculated values for regular end-on and side-on monolayers are marked as black dashed and dotted lines, according to the scheme in (e). The experiments are performed with a starting protein concentration of 2.0 mg ml^{-1} prior to *p*H adjustment.

about 50% (PAA_{TEM}) larger than on SiO_2, depending on the used normalization surface. This motivates an in-depth theoretical analysis of the adsorption modes at the atomistic level. In this section, static calculations are used to evaluate the force-distance profiles and predict the most favorable adsorption orientation of single protein molecules onto models of amorphous SiO_2 and TiO_2 surfaces at different *p*H values, according to Hildebrand *et al.*[93] To this aim, 36 different protein orientations are considered, giving rise to a broad interaction profile and revealing the most attractive orientation for each surface and *p*H (Fig. 9). For both surfaces, the protein/surface force profiles are largely defined by the interaction between the strong protein dipole moment and the charge distribution at the surface. For the case of SiO_2, an average attraction interaction (negative forces) is observed at all *p*H values, with an increased attraction and clearer dipole orientation while the *p*H increases and the surface become more and more negative. On TiO_2, on the other hand, repulsion is predicted at *p*H values lower than the surface IEP (6.0), whereas attraction takes place only at *p*H 7.4 and 8.0. Note also the inversion of the dipole moment in the most attractive (or least repulsive) protein orientation in passing from *p*H 5.0 to 7.4 (Fig. 9, left). At *p*H 8, in the most attractive orientation the protein faces the surface with its two α-helix motifs, and the enzymatically active site points sideways with respect to the surface normal.

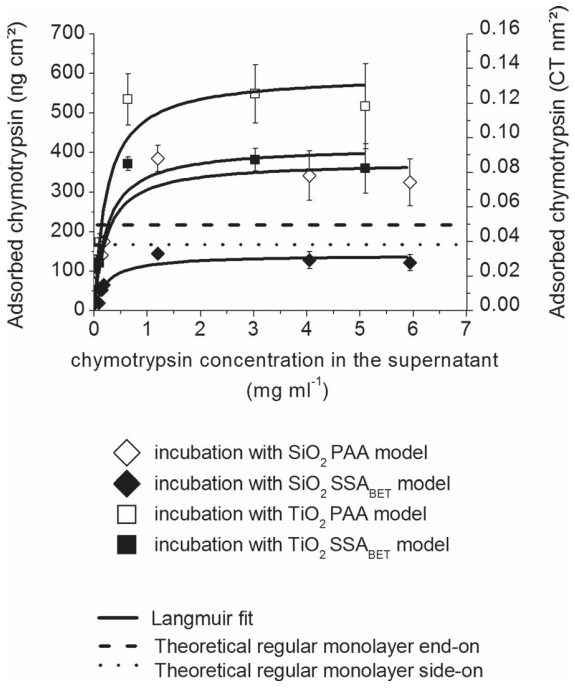

FIG. 8. Concentration-dependent adsorption of chymotrypsin on SiO_2 and TiO_2 colloidal particles at *p*H 8 after 20 h of incubation. The data are normalized with respect to the SSA_{BET} and PAA_{TEM} surface areas. Theoretically calculated values for regular monolayer in adsorption orientation end-on and side-on are marked as black dashed lines. The data shown represent means ± SD of values obtained in three independent experiments, and are fitted with a Langmuir isotherm model (black lines).

The maximum attractive forces are experienced by the protein at *p*H 8 at a height of about 1.5 nm over either surface. It has to be stressed that these calculations only take into account the DLVO interactions in a continuum-solvent approximation, and that further protein approach to the surface below 1.0 nm is strongly mediated by the structuring of the water molecules in surface proximity.[69,93,94] At this stage, it can be only concluded that long-range DLVO attraction is clearly evident at the larger *p*H values, which agrees with the measured trend of the adsorbed protein amount (Fig. 7), and that stronger attraction is experienced over SiO_2, which instead does not correlate with the experimental observation. The interaction profiles over TiO_2 are less deep and more narrow compared to SiO_2. One can thus expect an easier reorientation of chymotrypsin over TiO_2 because of a less distinct force dependence of the orientation.

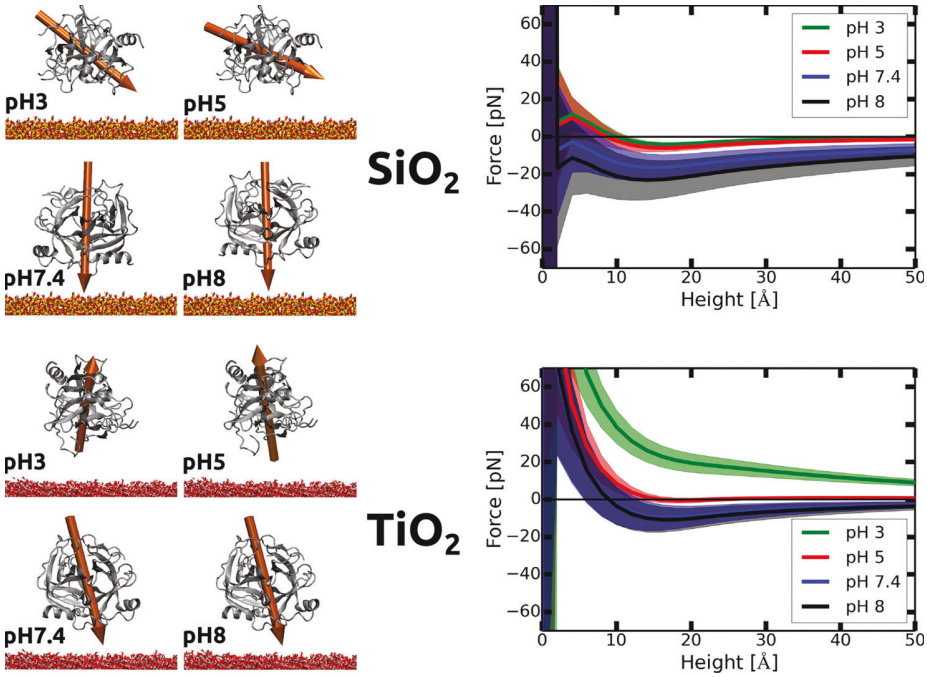

FIG. 9. (*Left*) Predicted most attractive orientations of chymotrypsin over SiO_2 and TiO_2 at different *p*H values. The molecular dipole moment is shown as an orange arrow. (*Right*) Force-height profiles calculated in implicit solvent for 36 different orientations at each *p*H value. The averages over all orientations are drawn with the bold colored lines, and the standard deviations are represented with semitransparent colored regions. Negative values define attractive forces. The height is defined as the distance in the surface normal direction between the highest surface atom and the lowest protein atom.

This is indeed confirmed by analyzing the relative energy changes upon rotation of the proteins around two independent axes at the constant height of 1.0 nm (Fig. 10). Here, at all considered *p*H values, a beltlike feature in the diagram can be observed, which corresponds to an orientation of the molecular dipole normal to the surface (in either direction), as discussed in detail in Hildebrand *et al.*[93] This interaction pattern is less distinct for smaller *p*H values. In the energy diagrams, the attraction or repulsion forces are shown with the small black arrows. The differences in the relative energy upon molecular reorientation are about 24 kcal mol^{-1} over SiO_2 and 12 kcal mol^{-1} over TiO_2.

G. Interaction forces for chymotrypsin multilayers

While Sec. III F has dealt with the case of a single protein approaching the surfaces, we consider here the presence of a preadsorbed protein monolayer, thus explicitly taking into account protein–protein interactions (Fig. 11). A first calculation is performed evaluating the relative energy changes associated with the reorientation of one protein within a preadsorbed protein monolayer [Fig. 11(a)] with a density of 0.034 molecule/nm^2 (corresponding to a theoretical end-on monolayer, see Fig. 7). Here, the protein height is fixed at 0.3 nm, and the map of energy changes obtained upon rotation around two axes is reported in Fig. 11(b) for the

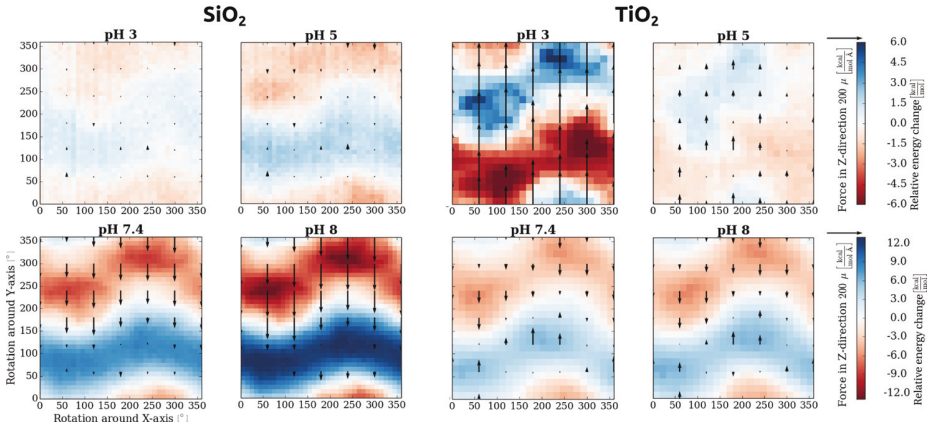

FIG. 10. Calculated relative energy changes associated with rotation of chymotrypsin at a height of 10 Å over the surfaces for (*left*) SiO_2 and (*right*) TiO_2, for four different *p*H values. The superimposed arrows represent the force values (downwards for attractive and upwards for repulsive forces).

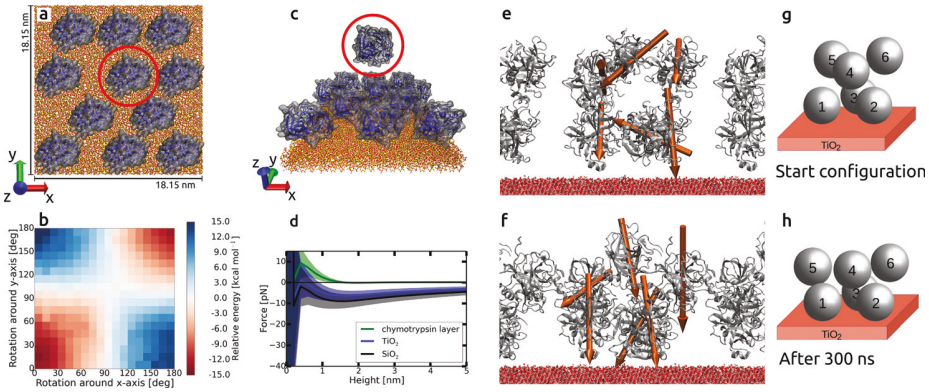

FIG. 11. Driving force for the formation of protein multilayers on SiO_2 and TiO_2. (a) Atomistic representation of an end-on monolayer at the density of 0.034 ± 0.001 molecules/nm^2. The red circle marks a protein which is rotated along two axis (x and y), giving rise to the energy map in (b). The force profiles calculated for an additional protein (c) interacting with the monolayer in the absence (green curve) or in the presence of surfaces (blue and gray curves) are shown in (d). Here, a height of zero is defined when the highest monolayer atom and the lowest atom of the additional protein are at the same height in the direction of the surface normal. (d) and (e) The initial and final configurations of a protein double layer (0.077 protein molecules nm^{-2}) on TiO_2 in an explicit-solvent MD simulation lasting 300 ns. (f) and (g) Schemes showing the protein positions in the double layers corresponding to (d) and (e).

representative case of SiO_2. A visually almost identical map is obtained for TiO_2. Starting from the most attractive adsorption orientation predicted for single proteins (at $x = y = 0$), rotation in any direction is associated with an energy increase, and an energy maximum is obtained for the molecular dipole pointing in the opposite direction ($x = 180$, $y = 0$; or $x = 0$, $y = 180$). The maximum is 30 kcal mol^{-1} higher than the minimum for the case of SiO_2 and 20 kcal mol^{-1} higher than the minimum for the case of TiO_2. This suggests that, in spite of the parallel arrangement of the molecular dipoles, in the most favorable configuration within a monolayer, all proteins are oriented in the same way, with their α-helices pointing toward the surface.

A second calculation is then performed to evaluate the force-distance profile associated with the approach of a single chymotrypsin molecule toward an already present protein monolayer either adsorbed on the two surfaces [Fig. 11(c)], or suspended in solution, as a reference. The resulting profiles averaged over 36 different protein orientations [Fig. 11(d)] revealed that *repulsion* is predicted in the absence of an underlying surface, thus suggesting no favorable driving force for spontaneous formation of protein agglomerates in solution. However, *attraction* is predicted for a monolayer on either SiO_2 or TiO_2, as a consequence of the strong interaction exerted by the surface, which is not completely shielded by the presence of an adsorbed monolayer. Also, in this case, attraction is slightly stronger for the case of SiO_2, and the most attractive protein orientation is as in the preformed monolayer.

To confirm that the attractive interactions may in fact lead to adsorption beyond one theoretical monolayer, a molecular dynamics simulation in explicit water solvent is performed starting from a double-layer configuration with randomly oriented proteins [Figs. 11(d) and 11(f)]. After 300 ns of simulation, we observe two mayor trends: first, on both surfaces, the proteins collectively move closer to the surface and form a more compact layer. Second, the individual proteins rotate toward the most-attractive orientation presented in Fig. 9 (*left*). In some cases, rotation is hindered by close protein–protein contacts, which remain stable for the whole simulation time [Figs. 11(e) and 11(g)].

In summary, the simulations presented in this section indicate the presence of both long- and short-range interactions leading to the formation of adsorbed layers with a protein concentration well beyond one theoretical monolayer, which agrees well with the experimental observation (cf. Figs. 7 and 8). However, these simulations are still not able to explain differences in the adsorption modes on SiO_2 and TiO_2 resulting in a larger amount of proteins adsorbed on TiO_2 than on SiO_2. To further explore this issue, explicit solvent MD simulations of adsorbed proteins are presented in Sec. III H.

H. Explicit-solvent MD simulations of chymotrypsin adsorption on TiO_2 and SiO_2

To analyze the atomistic details of the protein approach and adsorption on the two surfaces, we have performed MD simulations in explicit solvent at *p*H 8 following Hildebrand *et al.*[93] In the input structures, the protein is placed at a height of 10 Å in six different arbitrary orientations (Fig. 12). During the simulations, the protein spontaneously adsorb on the surface after about 5 ns and find a stable adsorption configuration, undergoing a rotation toward the most favorable orientation predicted by the implicit-solvent calculations [cf. Figs. 12(a) and 12(b) with Fig. 9]. The simulations are stopped after 50 ns.

The evolution of the protein–surface contacts during a representative simulation is shown in Figs. 12(c)–12(f). Here, a protein–surface contact is defined if the distance between one atom of the surface and one atom of the protein becomes less than 2.4 Å. For both surfaces, the most frequent binding motifs of the protein are the positively charged amino acid lysine as well as the polar amino acid threonine [Figs. 12(c)–12(d)]. The most common surface sites involved in the contacts are

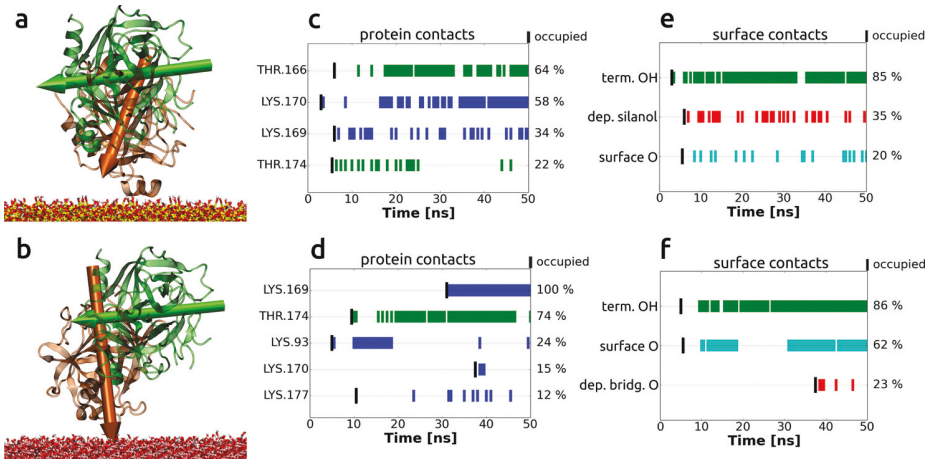

FIG. 12. [(a) and (b)] Initial (green arrow) and final (orange arrow) chymotrypsin orientations upon adsorption on (a) SiO_2 and (b) TiO_2 obtained in MD simulations in explicit water solvent. [(c)–(d)] Contact analysis of the protein residues for SiO_2 (c) and TiO_2 (d). The color code represents positively charged amino acids (blue) and polar amino acids (green). [(e) and (f)] Contact analysis for the surface residues of (e) SiO_2 and (f) TiO_2. The percentages reported at the right side of each subfigure indicate the occupancies over time after the first contact (marked with a bold black bar). Groups forming contacts for less than 10% of the time are not shown.

terminal OH groups both on SiO_2 and TiO_2. Deprotonated silanol groups play a very important role on SiO_2, whereas deprotonated O sites on TiO_2 are much less frequently involved. Neutral O sites are also present in the analysis, in larger proportion on TiO_2 than on SiO_2 [Figs. 12(e)–12(f)]. These differences could have their origin in the larger density of negatively charged surface groups present on silica, and are likely to influence the protein adsorption modes.

Differences in the adsorption behavior of the two proteins may be also related to their mobility after adsorption. To investigate this issue, we perform steered MD simulations in explicit solvent, in which the previously adsorbed protein is pulled parallel to the surfaces by means of a harmonic constraint applied to its center of mass (Fig. 13). The pulling velocity is 0.5 m/s, and the constraint force-constant is 1000 kJ $mol^{-1} nm^{-2}$. Two perpendicular pulling directions were chosen to alleviate direction-dependent effects, namely, the $\langle 100 \rangle$ and $\langle 010 \rangle$ directions of the simulation box. We stress that in these simulations the proteins are free to roll and/or slide over the surface, and even to desorb, since no constraint over the position, but only the velocity, of their centers of mass is applied.

The protein/surface contacts formed during these simulations (see supplementary Fig. S3) correspond to a large extent to those reported in Fig. 12, with the exception that on SiO_2 more amino acid types (including hydrophobic ones) are involved in surface binding. More interesting, however, is the analysis of the rolling/sliding behavior of the protein over the two surfaces, as reported in Fig. 13 and visible in supplementary material videos (SI Videos 1 to 4).

The force required to pulling the whole protein over the surface and the associated cumulative work is slightly larger for the SiO_2 surface. Especially in one simulation (pulling along $\langle 100 \rangle$ on TiO_2), the negligibly small force and work result from temporary desorption of the protein between 5 and 15 ns. A striking difference lies in the fact that the protein tends to roll over SiO_2, while it tends to slide over TiO_2. This is visible from the evolution of the angle between the molecular dipole moment and the direction normal to the surface and especially from its time derivative, as shown in Fig. 13. For SiO_2, the angle varies more continuously toward smaller and smaller values, and the angle derivative is most of the time negative, indicating progressive rolling. This is noteworthy if one takes into account that rotation of the dipole is associated with a considerable increase in the amount of potential energy [see Figs. 11(a) and 11(b)]. For TiO_2, the derivative of the angle tends to oscillate around zero, indicative of predominant sliding.

Further differences in the adsorption modes of chymotrypsin on the SiO_2 and TiO_2 surfaces are highlighted through the calculation of the radial distribution function (RDF) between selected pairs of all atoms of the surface, the water solvent, and the protein (Fig. 14). Water molecules are known to form shell-like structures around hydrophilic surface terminal groups.[93] The RDF of water around all surface atoms shows a less distinct structuring on SiO_2 (Fig. 14, *top left*) compared to the very evident structuring in two hydration layers on TiO_2 (Fig. 14, *top right*). As far as the protein is concerned, the RDF shows that hydrophobic residues are in close contact (within the first 4 Å) to the surface in the case of silica, whereas only hydrophilic residues are in direct contact with titania. Interesting is the small peak of the SiO_2 protein–surface RDF at about 1.5 Å, i.e., before the first peak of the water-surface RDF (at 1.8 Å), indicating that some protein residues are able to deeply penetrate the first hydration layer and very tightly bind to surface sites. As already shown by the temporary evolution of the contacts (Fig. 12), the positively charged lysine and arginine residues are abundantly present close to deprotonated silanol groups on SiO_2, and present only to a minor extent around deprotonated bridging oxygen on TiO_2.

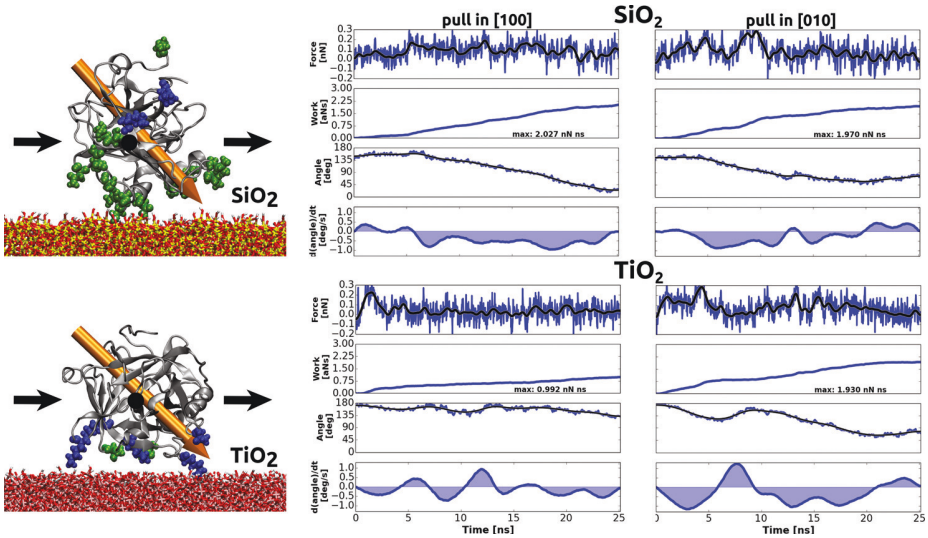

FIG. 13. (*Left*) Initial configurations of steered MD simulations of chymotrypsin pulled over the SiO_2 and TiO_2 surfaces. (*Right*) Time evolutions along the corresponding trajectories of the constrained force, the cumulative work, the angle of the dipole moment to the surface normal, and its time derivative (from top to bottom in each panel) for SiO_2 (top) and TiO_2 (bottom). The protein is pulled in each case along the ⟨100⟩ and ⟨010⟩ directions of the simulation box.

IV. DISCUSSION AND CONCLUSIONS

Motivated by the need to optimize the conditions leading to maximum adsorption of chymotrypsin on colloidal ceramic supports, we have performed a comparative study of the adsorption features of the protein on highly pure SiO_2 and TiO_2 colloidal particles combining adsorption experiments with all-atom MD simulations. The analysis has revealed some common features, such as the same preferred adsorption orientation on the two materials at neutral and basic *p*H driven by interaction of the negatively charged surfaces with the strong protein dipole moment (Fig. 9). Moreover, a nearly equal free energy of adsorption in the low-concentration limits (about −35 kJ/mol) has been estimated by the Langmuir adsorption isotherm analysis (Fig. 8). However, a number of differences have also been identified, which we believe to be responsible for the experimentally observed larger amount of adsorbed proteins found on TiO_2 than on SiO_2 (Figs. 7 and 8).

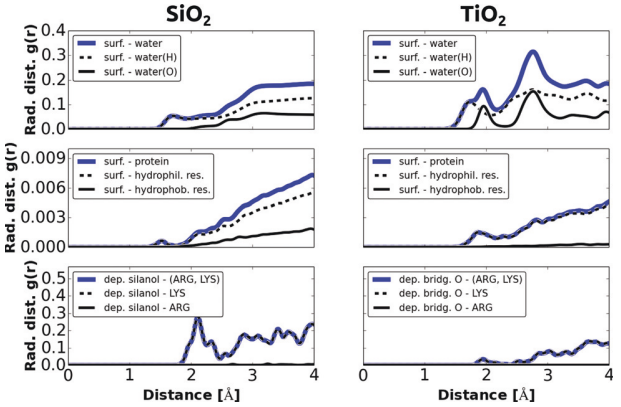

FIG. 14. Radial distribution function (RDF) of selected pairs of atoms for chymotrypsin adsorbed and pulled over SiO_2 (left) and TiO_2 (right): (top) surface-water RDF; (middle) surface–protein RDF, separating the contributions of hydrophilic and hydrophobic residues. (Bottom) RDF between positively charged amino acids with negatively charged surface sites.

Anchoring to the SiO_2 surface (IEP ∼2.7) takes place mostly via positively charged amino acids that interact with both neutral and deprotonated silanol groups. However, also other neutral polar and even hydrophobic residues contribute to frequent and tight surface–protein contacts (see Figs. 12 and 14, and Ref. 93). Anchoring to the TiO_2 surface (IEP ∼6.6), which presents a smaller density of deprotonated sites at the *p*H values relevant to adsorption (7.4 and 8.0), is rather dominated by neutral terminal OH and bridging O sites, although involving almost exclusively positively charged amino acids. We believe that the distinct structuring of the surface hydration layers in which the amino acids are embedded (see Fig. 14) effectively compensates for the absence of direct ionic interactions between protein and surface, so that, overall, the free energy of binding to either surface is nearly the same. Different, however, is the ability of the protein to diffuse over the surface once tightly adsorbed. Our steered MD simulations (Fig. 13) reveal that chymotrypsin can easily slide over the TiO_2 surface, and even temporarily desorb and adsorb again at a farther site. On the contrary, no temporary desorption is observed from the SiO_2 surface, also consistently with the larger attraction forces predicted by our static calculations (Fig. 9). In this case, rupture of the tight surface–protein contacts only takes place if new contacts are concomitantly formed, resulting in a predominant rolling behavior. A change in the dipole orientation due to rolling, in turn, is associated with a considerable energy loss [see Figs. 10, 11(a), and 11(b)], so that diffusion over the SiO_2 surface is expected to be more hindered than diffusion over the TiO_2 surface.

Considering these arguments, it is possible to rationalize both why a larger maximum adsorption amount is reached on TiO_2 (Figs. 7 and 8) and why reaching the maximum

adsorption amount is slower on SiO_2 (Fig. 7), so that adsorption equilibrium is obtained only after 16–20 h of incubation. While our simulations clearly show that at least a double monolayer is energetically stable on either surface (Fig. 10), its actual formation relies on diffusion of preadsorbed proteins to accommodate new ones from the solution. This process is probably easier on TiO_2 because of the observed more favorable diffusion mobility.

A crucial point to consider in the analysis of the protein adsorption amount is the normalization with respect to the available surface area of the particles. Traditionally, the particle surface area is measured by means of N_2 adsorption at low temperature and fitting of the data with the BET adsorption isotherm.[32–34,95] The so-obtained SAA_{BET} therefore represents an N_2-accessible surface, which includes the cavity walls of micropores (with diameters of the order of 2 nm or smaller) possibly present on the particle surfaces. Such pores are not accessible by chymotrypsin, which has a diameter of about 5 nm (Fig. 1). Notably, reports about the presence of microporosity in Stöber silica are not uncommon.[86,87] Because of this reason, we have also normalized the experimental data with respect to a here-defined protein accessible area, estimated from a geometrical analysis of the particles imaged by TEM (PAA_{TEM}). In doing this, the difference in the maximum protein amount adsorbed on TiO_2 and SiO_2 is reduced from a factor of 3 to a factor of 1.5. This is more consistent with the rather subtle differences in the adsorption behavior observed in the MD simulations. Moreover, only after PAA_{TEM} normalization do the data suggest formation of a double protein monolayer also on SiO_2. Instead, the SSA_{BET} normalization would predict formation of barely a single monolayer (Fig. 7), in striking contrast with the driving force for double monolayer formation emerging from all simulations.

The presence of micropores in the employed SiO_2 particles would easily explain the much larger amount of adsorbed water with respect to TiO_2 (Fig. 4), and also the hysteresis observed in the water adsorption/desorption curves, which could be caused by trapping of water molecules within the micropores due to steric and capillary effects. Notably, the adsorption isotherm of heptane (a larger molecule that probably does not enter into the smaller micropores) reveals slightly reduced adsorption on SiO_2 with respect to TiO_2 and no appreciable hysteresis. It shall be noted, however, that unexpected high hydrophobicity could also be due to surface contaminants not removed by calcination (e.g., a small amount of pyrolytic carbon).

We finally note that a precise determination of the surface area accessible to protein adsorption is also complicated by the tendency of the particles to form agglomerates, especially in the case of TiO_2, which is less charged at neutral *p*H and presents a larger Hamaker constant than SiO_2. Agglomeration also prevents the use of DLS radii to estimate the actual size (and thus the surface area) of the particles. Therefore, a careful pretreatment with ultrasound is absolutely necessary prior to each incubation and adsorption study, and the possibility of reagglomeration needs to be taken into account when performing experiments with long incubation times.

Future studies shall focus on the conformational changes that the protein may undergo after adsorption, and may severely influence its enzymatic activity.[59,92] Also, in this case, a combination of experimental studies (e.g., by means of circular dichroism spectroscopy) and molecular dynamics simulations would be desirable in order to achieve a comprehensive description of the protein's behavior at the atomic scale.

ACKNOWLEDGMENTS

The authors thank Katharina Richter and Klaus Rischka [Fraunhofer Institute for Manufacturing Technology and Advanced Materials (IFAM) in Bremen] for technical support with the MALDI ToF-MS experiments. This work was funded by the Deutsche Forschungsgemeinschaft under Grant Nos. KO3811|3-1, CI144/2 (Emmy Noether Program), and by the State of Bremen through the APF Programme "Keramische Grenzflächentechnologie." Computational resources were provided by the North-German Supercomputing-Alliance system (HLRN).

[1]R. K. Singh, M. K. Tiwari, R. Singh, and J. K. Lee, Int. J. Mol. Sci. **14**, 1232 (2013).
[2]R. A. Sheldon and S. van Pelt, Chem. Soc. Rev. **42**, 6223 (2013).
[3]R. C. Rodrigues, C. Ortiz, A. Berenguer-Murcia, R. Torres, and R. Fernandez-Lafuente, Chem. Soc. Rev. **42**, 6290 (2013).
[4]D. Brady and J. Jordaan, Biotechnol. Lett. **31**, 1639 (2009).
[5]U. Hanefeld, L. Q. Cao, and E. Magner, Chem. Soc. Rev. **42**, 6211 (2013).
[6]C. Mateo, J. M. Palomo, G. Fernandez-Lorente, J. M. Guisan, and R. Fernandez-Lafuente, Enzyme Microb. Technol. **40**, 1451 (2007).
[7]M. C. R. Franssen, P. Steunenberg, E. L. Scott, H. Zuilhof, and J. P. M. Sanders, Chem. Soc. Rev. **42**, 6491 (2013).
[8]M. Hartmann and X. Kostrov, Chem. Soc. Rev. **42**, 6277 (2013).
[9]A. Liese and L. Hilterhaus, Chem. Soc. Rev. **42**, 6236 (2013).
[10]S. Andreescu, J. Njagi, and C. Ispas, "Nanostructured materials for enzyme immobilization and biosensors," in *The New Frontiers of Organic and Composite Nanotechnology*, edited by V. Erokhin, M. K. Ram, and O. Yavuz (Elsevier, Amsterdam, 2008), Chap. 7, p. 355.
[11]S. A. Bhakta, E. Evans, T. E. Benavidez, and C. D. Garcia, Anal. Chim. Acta **872**, 7 (2015).
[12]J. Krenkova and F. Svec, J. Sep. Sci. **32**, 706 (2009).
[13]A. Monzo, E. Sperling, and A. Guttman, TrAC, Trends Anal. Chem. **28**, 854 (2009).
[14]*Bioconjugate Techniques*, edited by G. T. Hermanson (Elsevier, Amsterdam, 2008).
[15]E. A. Ponomareva, V. E. Kartuzova, E. G. Vlakh, and T. B. Tennikova, J. Chromatogr. B **878**, 567 (2010).
[16]J. L. Brash and P. W. Wojciechowski, *Interfacial Phenomena and Bioproducts* (Marcel Dekker, New York, 1996), p. xi.
[17]S. A. Ansari and Q. Husain, Biotechnol. Adv. **30**, 512 (2012).
[18]D. H. Chen and R. A. Caruso, Adv. Funct. Mater. **23**, 1356 (2013).
[19]M. De, P. S. Ghosh, and V. M. Rotello, Adv. Mater. **20**, 4225 (2008).
[20]A. Elaissari, *Colloidal Nanoparticles in Biotechnology* (Wiley-Interscience, Hoboken, NJ, 2008), p. xiii.
[21]F. M. K. Tehrani, M. Rashidzadeh, A. Nemati, A. Irandoukht, and B. Faridnia, Int. J. Environ. Sci. Technol. **8**, 545 (2011).
[22]L. Treccani, T. Y. Klein, F. Meder, K. Pardun, and K. Rezwan, Acta Biomater. **9**, 7115 (2013).
[23]S. An, M. W. Lee, B. N. Joshi, A. Jo, J. Jung, and S. S. Yoon, Ceram. Int. **40**, 3305 (2014).
[24]S. K. Das, M. M. R. Khan, T. Parandhaman, F. Laffir, A. K. Guha, G. Sekarana, and A. B. Mandal, Nanoscale **5**, 5549 (2013).

[25]V. Likodimos, D. D. Dionysiou, and P. Falaras, Rev. Environ. Sci. Bio/Technol. **9**, 87 (2010).
[26]J. B. Liu, Z. M. Wang, Z. P. Luo, and S. Bashir, Dalton Trans. **42**, 2158 (2013).
[27]A. Sharif, H. Koolivand, G. Khanbabaie, M. Hemmati, J. Aalaie, M. R. Kashani, and A. Gheshlaghi, J. Polym. Res. **19**, 9916 (2012).
[28]F. De Persiis, C. La Mesa, and R. Pons, Soft Matter **8**, 1361 (2012).
[29]Q. J. He and J. L. Shi, J. Mater. Chem. **21**, 5845 (2011).
[30]H. D. Jang, D. S. Kil, H. Chang, K. Cho, S. K. Kim, K. J. Oh, and J. H. Choi, J. Nanosci. Nanotechnol. **11**, 4169 (2011).
[31]W. Norde and C. E. Giacomelli, J. Biotechnol. **79**, 259 (2000).
[32]W. Norde and T. Zoungrana, Biotechnol. Appl. Biochem. **28**, 133 (1998).
[33]T. Zoungrana, G. H. Findenegg, and W. Norde, J. Colloid Interface Sci. **190**, 437 (1997).
[34]K. Rezwan, L. P. Meier, and L. J. Gauckler, Biomaterials **26**, 4351 (2005).
[35]R. S. Rao, P. S. Borkar, C. N. Khobragade, and A. D. Sagar, Enzyme Microb. Technol. **39**, 958 (2006).
[36]R. W. Ammann, E. Tagwecher, H. Kashiwagi, and H. Rosenmund, Am. J. Dig. Dis. **13**, 123 (1968).
[37]M. A. Remtulla, P. R. Durie, and D. M. Goldberg, Clin. Biochem. **19**, 341 (1986).
[38]M. Wald, T. Olejar, V. Sebkova, M. Zadinova, M. Boubelik, and P. Pouckova, Cancer Chemother. Pharmacol. **47**, S16 (2001).
[39]H.-J. R. Butt and M. Kappl, *Surface and Interfacial Forces* (Wiley-VCH, Weinheim, 2010), p. xv.
[40]R. R. Zhu, W. R. Wang, X. Y. Sun, H. Liu, and S. L. Wang, Toxicol. In Vitro **24**, 1639 (2010).
[41]F. Meder, T. Daberkow, L. Treccani, M. Wilhelm, M. Schowalter, A. Rosenauer, L. Madler, and K. Rezwan, Acta Biomater. **8**, 1221 (2012).
[42]A. A. Thyparambil, Y. Wei, and R. A. Latour, Biointerphases **10**, 019002 (2015).
[43]W. Norde, Adv. Colloid Interface **25**, 267 (1986).
[44]P. Maffre, K. Nienhaus, F. Amin, W. J. Parak, and G. U. Nienhaus, Beilstein J. Nanotechnol. **2**, 374 (2011).
[45]C. Rocker, M. Potzl, F. Zhang, W. J. Parak, and G. U. Nienhaus, Nat. Nano **4**, 577 (2009).
[46]P. B. Welzel, Thermochim. Acta **382**, 175 (2002).
[47]*Studies in Interface Science*, edited by A. S. Dukhin and P. J. Goetz (Elsevier, Amsterdam, 2002), Vol. 15.
[48]P. C. Hidber, "Zusammenhang von Struktur und Wirkung von Carbonsäuren als Verflüssiger für wässrige α-Aluminiumoxidsuspensionen," Ph.D. thesis (ETH Zurich Switzerland, Zurich, 1993).
[49]See supplementary material at http://dx.doi.org/10.1116/1.4940701 for Figs. S1 (TEM images of nanoparticles to determine their representative geometrical size); S2 (MALDI-ToF-MS spectra of chymotrypsin reference solutions in the range of 800–3500 Da/e); S3 (Analysis of the chymotrypsin–surface contacts in the constrained simulations); Four videos showing the trajectories of the constrained simulations of chymotrypsin pulled over each surface in two different directions.
[50]H. D. Ackler, R. H. French, and Y. M. Chiang, J. Colloid Interface Sci. **179**, 460 (1996).
[51]A. L. Gomez-Merino, F. J. Rubio-Hernandez, J. F. Velazquez-Navarro, F. J. Galindo-Rosales, and P. Fortes-Quesada, J. Colloid Interface Sci. **316**, 451 (2007).
[52]S. J. Compton and C. G. Jones, Anal. Biochem. **151**, 369 (1985).
[53]A. H. Reisner, P. Nemes, and C. Bucholtz, Anal. Biochem. **64**, 509 (1975).
[54]P. K. Smith *et al*., Anal. Biochem. **150**, 76 (1985).
[55]K. J. Wiechelman, R. D. Braun, and J. D. Fitzpatrick, Anal. Biochem. **175**, 231 (1988).
[56]K. K. Ghosh and S. K. Verma, Indian J. Biochem. Biophys. **45**, 350 (2008).
[57]S. Kumar, K. Dar, S. Ganno, and H. Hatano, J. Biol. Chem. **250**, 5393 (1975).
[58]C. I. Mekras, M. H. George, and J. A. Barrie, Int. J. Biol. Macromol. **11**, 113 (1989).
[59]L. Derr, R. Dringen, L. Treccani, N. Hildebrand, L. C. Ciacchi, and K. Rezwan, J. Colloid Interface Sci. **455**, 236 (2015).
[60]R. Dringen, Y. Koehler, L. Derr, G. Tomba, M. M. Schmidt, L. Treccani, L. C. Ciacchi, and K. Rezwan, Langmuir **27**, 9449 (2011).
[61]A. P. Serro, K. Degiampietro, R. Colaco, and B. Saramago, Colloid Surf., B **78**, 1 (2010).
[62]E. Jones *et al*., SciPy: Open Source Scientific Tools for Python, 2001, see: http://www.scipy.org/.
[63]D. A. Case *et al*., J. Comput. Chem. **26**, 1668 (2005).
[64]P. A. Frey, S. A. Whitt, and J. B. Tobin, Science **264**, 1927 (1994).
[65]H. Caldararu, G. S. Timmins, M. J. Davies, and B. C. Gilbert, J. Chem. Soc. Faraday Trans. **92**, 3151 (1996).
[66]S. Demaneche, J. P. Chapel, L. J. Monrozier, and H. Quiquampoix, Colloid Surf., B **70**, 226 (2009).
[67]N. Ui, Biochim. Biophys. Acta **229**, 582 (1971).
[68]W. L. Jorgensen, J. Chandrasekhar, J. D. Madura, R. W. Impey, and M. L. Klein, J. Chem. Phys. **79**, 926 (1983).
[69]D. J. Cole, M. C. Payne, G. Csanyi, S. M. Spearing, and L. Colombi Ciacchi, J. Chem. Phys. **127**, 204704 (2007).
[70]A. Butenuth, G. Moras, J. Schneider, M. Koleini, S. Köppen, R. Meißner, L. B. Wright, T. R. Walsh, and L. C. Ciacchi, Phys. Status Solidi B **249**, 292 (2012).
[71]Anon, *The Surface Properties of Silicas*, edited by A. P. Legrand (Wiley, Chichester, 1998).
[72]P. M. Dove and C. M. Craven, Geochim. Cosmochim. Acta **69**, 4963 (2005).
[73]M. Kobayashi, F. Juillerat, P. Galletto, P. Bowen, and M. Borkovec, Langmuir **21**, 5761 (2005).
[74]J. Sonnefeld, A. Göbel, and W. Vogelsberger, Colloid Polym. Sci. **273**, 926 (1995).
[75]S. Salameh, J. Schneider, J. Laube, A. Alessandrini, P. Facci, J. W. Seo, L. C. Ciacchi, and L. Madler, Langmuir **28**, 11457 (2012).
[76]T. Hiemstra, J. C. M. De Wit, and W. H. Van Riemsdijk, J. Colloid Interface Sci. **133**, 105 (1989).
[77]S. Köppen and W. Langel, Surf. Sci. **600**, 2040 (2006).
[78]J. Schneider and L. C. Ciacchi, Surf. Sci. **604**, 1105 (2010).
[79]J. Schneider and L. C. Ciacchi, J. Chem. Theory Comput. **7**, 473 (2010).
[80]A. Onufriev, D. Bashford, and D. A. Case, Proteins **55**, 383 (2004).
[81]S. Pronk *et al*., Bioinformatics **29**, 845 (2013).
[82]B. Hess, J. Chem. Theory Comput. **4**, 116 (2007).
[83]G. Bussi, D. Donadio, and M. Parrinello, J. Chem. Phys. **126**, 014101 (2007).
[84]W. Humphrey, A. Dalke, and K. Schulten, J. Mol. Graph Modell. **14**, 33 (1996).
[85]W. Kabsch and C. Sander, Biopolymers **22**, 2577 (1983).
[86]S. Li, Q. Wan, Z. Qin, Y. Fu, and Y. Gu, Langmuir **31**, 824 (2015).
[87]A. Mitra, A. Bhaumik, and T. Imae, J. Nanosci. Nanotechnol. **4**, 1052 (2004).
[88]B. M. C. Chan and J. L. Brash, J. Colloid Interface Sci. **84**, 263 (1981).
[89]J. L. Brash and Q. M. Samak, J. Colloid Interface Sci. **65**, 495 (1978).
[90]H. Y. Ju, C. H. Kuo, J. R. Too, H. Y. Huang, Y. K. Twu, C. M. J. Chang, Y. C. Liu, and C. J. Shieh, J. Mol. Catal. B: Enzym. **78**, 9 (2012).
[91]B. U. Specht and W. Brendel, Biochim. Biophys. Acta **484**, 109 (1977).
[92]L. Derr, S. Steckbeck, R. Dringen, L. Colombi Ciacchi, L. Treccani, and K. Rezwan, Anal. Lett. **48**, 424 (2014).
[93]N. Hildebrand, S. Köppen, L. Derr, K. Li, M. Koleini, K. Rezwan, and L. Colombi Ciacchi, J. Phys. Chem. C **119**, 7295 (2015).
[94]J. Schneider and L. Colombi Ciacchi, J. Am. Chem. Soc. **134**, 2407 (2012).
[95]A. Bentaleb, V. Ball, Y. Haikel, J. C. Voegel, and P. Schaaf, Langmuir **13**, 729 (1997).